were analyzed by SDS-PAGE and the Coomassie blue staining (Fig. 3B). Western blot analysis of Naf1(N) protein fragments using anti-myc antibody and the purified MAb shows that protein fragments were thoroughly produced in *E. coli*, and the epitope detected by the MAb was located at the overlapping region of protein fragments 1 and 2, between amino acid residues 64 and 88 (Fig. 3C).

We again constructed Naf1 fusion protein fragments (Fig. 3A–C) with overlapping regions between amino acid residues 64 and 88 (Fig. 3D). Expression of Naf1(N) protein fragments was ascertained by SDS-PAGE, followed by Coomassie blue staining (Fig. 3E) and Western blot analysis using anti-myc antibody (Fig. 3F). According to the result of Western blot analysis using anti-Naf1 MAb, as shown in Figure 3F, the MAb was found to have a specific binding ability to Naf1(N) fragment C. These results indicate that the epitope recognized by anti-Naf1 MAb was located at the amino acid residues 81–88 region of Naf1.

Endogenous Naf1 expression and subcellular localization

The ability of the anti-Naf1 MAb to detect endogenous Naf1 in various cells was also investigated by Western blot analysis and the immunofluorescent staining of cells followed by confocal microscopy (Fig. 4A,B). Cell lysates of unstimulated human PBL, Jurkat, MT-4, Molt 4, 293, and U-937 cells were applied to 12% gel SDS-PAGE, and immunoblotting with Naf1 MAb showed endogenous Naf1 protein with the molecular weight of about 72 kDa (Fig. 4A). Immunofluorescent staining of human PBL, Jurkat, MT-4, and Molt-4 cells with anti-Naf1 MAb, followed by the assess-

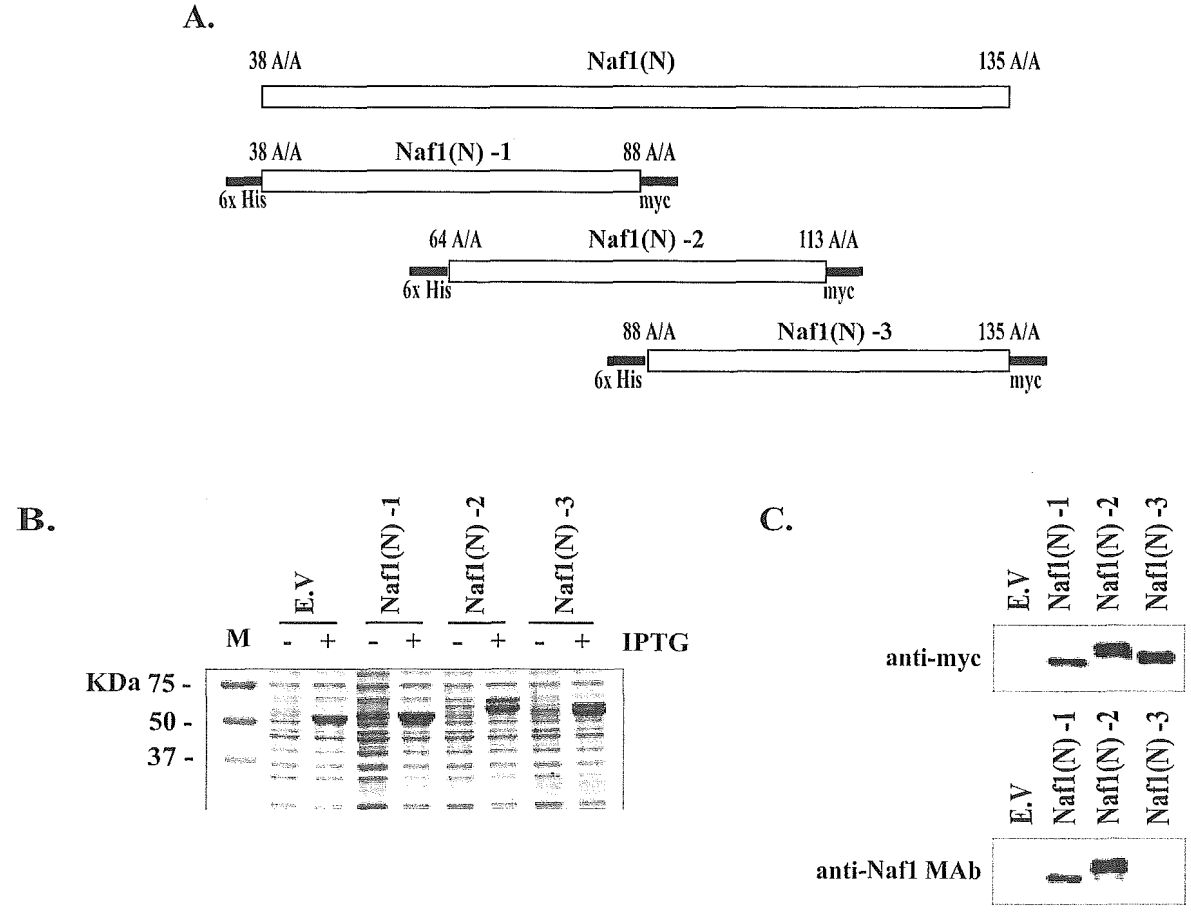

(continued)

FIG. 3. Mapping of the Naf1 epitope recognized by anti-Naf1 monoclonal antibody (MAb). (**A,D**) Schematic representation of N-terminally truncated Naf1 fusion proteins. The fusion proteins contain 6×His tag at N-terminus and myc tag at C-terminus. The numbers refer to the position of amino acids in Naf1 protein. (**B,E**) Sodium dodecyl sulfate–polyacrylamide gel electrophoresis (SDS-PAGE) and Coomassie Brilliant Blue staining for the expression of Naf1 fusion proteins from un-induced (−) or isopropyl-D-thiogalactopyranoside (IPTG) induced (+) *E. coli*, transformed with control empty vector (EV) or with pMAL-6×His-Naf1-myc cDNAs. (**C,F**) Western blot analysis of induced bacterial lysates expressing Naf1 fusion proteins. Lysates of induced *E. coli* were electrophoresed in 12% acrylamide gels and immunoblotted with anti-Naf1 MAb for the specific epitope (upper panels) or anti-myc MAb for the protein input control (lower panels).

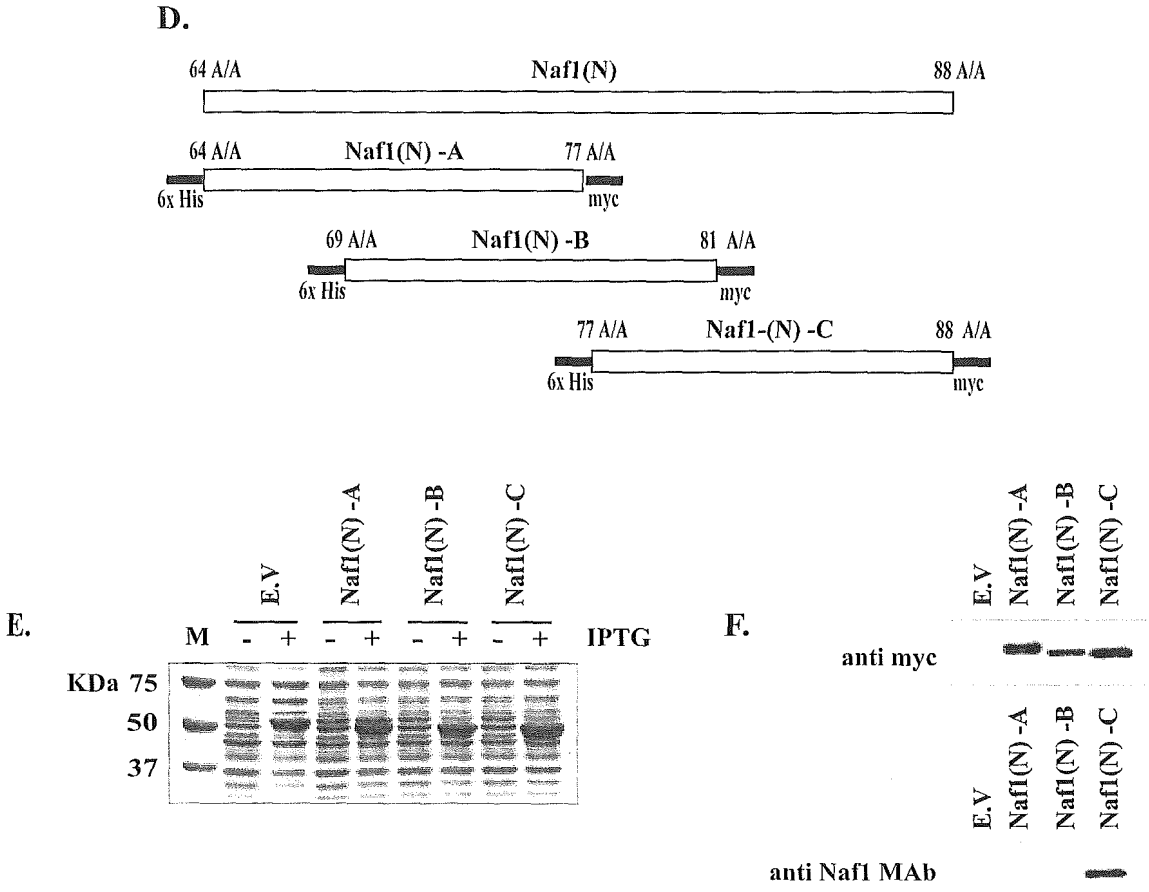

FIG. 3. *Continued.*

ment under confocal microscope, showed predominantly cytoplasmic localization of endogenous Naf1 (Fig. 4B).

DISCUSSION

In this report, we present the production and characterization of an MAb specific for the cellular protein, Naf1/ABIN-1. We used the baculovirus expression system to synthesize recombinant Naf1(N) protein. High Five cells were described to achieve higher protein production when compared with Sf9 cells.[30] Previous reports showed that hexahistidine tagging takes advantage of a high affinity to Ni-NTA resin in the purification procedure and does not interfere with the protein function.[29]

The ability of anti-Naf1 MAb to recognize endogenous Naf1 protein in various cell lines was examined by Western blotting and immunostaining. We also investigated the expression and localization of endogenous Naf1 in human PBL and other cell lines showing its cytoplasmic localization. According to previous reports, Naf1 associates with HIV-1 viral proteins, Nef, and matrix in the yeast two-hybrid system and pull-down assays using Naf1-overexpressed cell lysates.[1,2] HIV-1 Nef contributes substantially to AIDS pathogenesis by augmenting virus replication and markedly perturbing the T cell functions. Host cell activation by viral protein Nef has been supposed to be a result of interaction between Nef with cellular protein Naf1, which is involved in the signal transduction of host cells. Naf1 has also been known to interact with A20 zinc finger protein, previously characterized as an inhibitor of NF-κB activation and apoptosis. Naf1 (ABIN-1) has been reported to inhibit NF-κB–dependent gene expression induced by TNF and IL-1. Naf1 blocks NF-κB activation by negative feedback regulation of NF-κB, and it has also been suggested that Naf1 has the potential to inhibit TNF-induced activation of NF-κB upon overexpression.[24,26] However, most of these earlier experiments were performed with Naf1-overexpressed cells because of the lack of specific MAb to the endogenous Naf1. To investigate the Naf1-interacting proteins and their molecular functions under physiological condition, anti-Naf1 MAb is required to access endogenous Naf1 in some specific examinations, such as immunoprecipitation and immunostaining assays. The improvement in understanding of the activation and regulation of NF-κB has opened the way for the development of new treatments in inflammatory diseases as well

as in HIV infection. From a therapeutic point of view, genetic engineering of specific human cells to express an NF-κB inhibitor such as Naf1 will offer a novel therapeutic tool in gene therapy.

In conclusion, anti-Naf1 MAb will be an indispensable tool in various immunoassay and functional investigations concerning the endogenous Naf1. We hope this MAb may lead to new findings and understanding of Naf1 in many aspects relating to HIV infection and various inflammatory diseases in human beings.

ACKNOWLEDGMENTS

We thank Dr. Kazuo Terashima and Masami Koushi for their excellent technical assistance in immunostaining and confocal

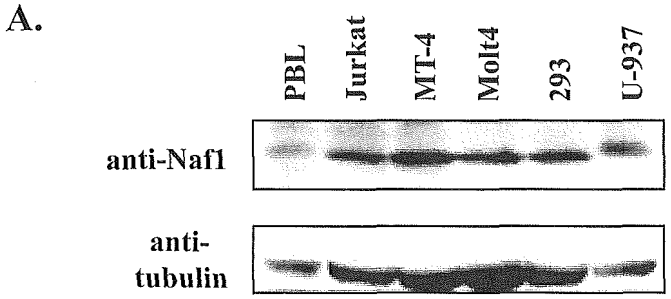

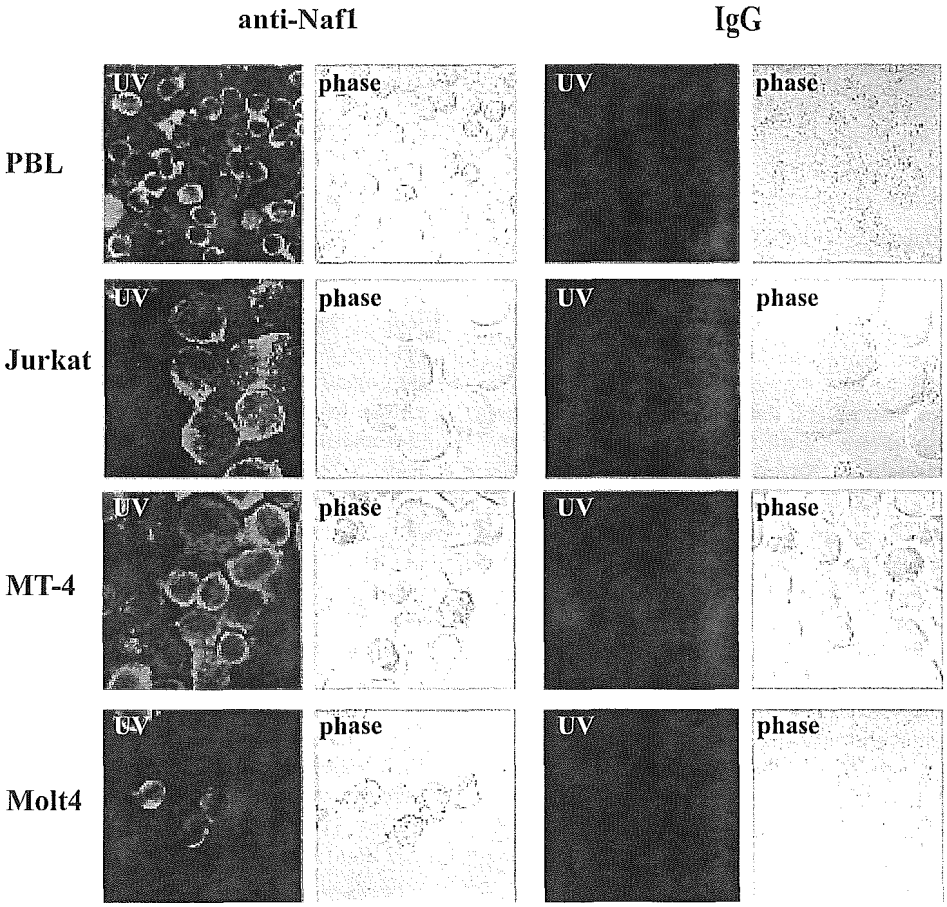

FIG. 4. Naf1 expression in human PBL, Jurkat, MT-4, Molt-4, 293, and U-937 cell lines. (**A**) Sodium dodecyl sulfate–polyacrylamide gel electrophoresis (SDS-PAGE) and Western blot analysis of cell lysates for the expression of endogenous Naf1 using anti-Naf1 monoclonal antibody (MAb). (**B**) Subcellular localization of Naf1 in human PBL, Jurkat, MT-4, and Molt-4 cells by immunofluorescence staining with anti-Naf1 MAb or control IgG and assessment under confocal microscopy.

microscopy. This work was supported by grants from the Ministry of Education, Science and Culture, and the Ministry of Health, Labor and Welfare of Japan.

REFERENCES

1. Fukushi M, Dixon J, Kimura T, Tsurutani N, Michael Dixon M, and Yamamoto N: Identification and cloning of a novel cellular protein Naf1, Nef-associated factor 1, that increases cell surface CD4 expression. FEBS Lett 1999;442:83–88.
2. Gupta K, Ott D, Hope TJ, Siliciano RF, and Boeke JD: A Human nuclear shuttling protein that interacts with human immunodeficiency virus type 1 matrix is packed into virions. J Virol 2000;74: 11811–11824.
3. Kestler HW 3rd, Ringler DJ, Mori K, Panicali DL, Sehgal PK, Daniel MD, and Desrosiers RC: Importance of the nef gene for maintenance of high virus loads and for development of AIDS. Cell 1991;65:651–662.
4. Miller MD, Warmerdam MT, Gaston I, Greene WC, and Feinberg MB: The human immunodeficiency virus–1 nef gene product: a positive factor for viral infection and replication in primary lymphocytes and macrophages. J Exp Med 1994;179: 101–113.
5. Spina CA, Kwoh TJ, Chowers MY, Guatelli JC, and Richman DD: The importance of nef in the induction of human immunodeficiency virus type 1 replication from primary quiescent CD4 lymphocytes. J Exp Med 1994;179:115–123.
6. Chowers MY, Spina CA, Kwoh TJ, Fitch NJ, Richman DD, and Guatelli JC: Optimal infectivity *in vitro* of human immunodeficiency virus type 1 requires an intact nef gene. J Virol 1994; 68:2906–2914.
7. Harris M: From negative factor to a critical role in virus pathogenesis: the changing fortunes of Nef J Gen Virol 1996;77:2379–2392.
8. Kawano Y, Tanaka Y, Misawa N, Tanaka R, Kira JI, Kimura T, Fukushi M, Sano K, Goto T, Nakai M, Kobayashi T, Yamamoto N, and Koyanagi Y: Mutational analysis of human immunodeficiency virus type 1 (HIV-1) accessory genes: requirement of a site in the nef gene for HIV-1 replication in activated $CD4^+$ T cells *in vitro* and *in vivo*. J Virol 1997;71:8456–8466.
9. Cullen BR: HIV-1 auxiliary proteins: making connections in a dying cell. Cell 1998;93:685–692.
10. Joseph AM, Kumar M, and Mitra D: Nef: "necessary and enforcing factor" in HIV infection. Curr HIV Res 2005;3:87–94.
11. Kirchhoff F, Greenough TC, Brettler DB, Sullivan JL, and Desrosiers RC: Absence of intact nef sequences in a long-term survivor with nonprogressive HIV-1 infection. N Engl J Med 1995; 332:228–232.
12. Piguet V, Chen YL, Mangasarian A, Foti M, Carpentier JL, and Trono D: Mechanism of Nef-induced CD4 endocytosis: Nef connects CD4 with the μ chain of adaptor complexes. EMBO J 1998; 17:2472–2481.
13. Kim YH, Chang SH, Kwon JH, and Rhee SS: HIV-1 Nef plays an essential role in two independent processes in CD4 down-regulation: dissociation of the CD4–$p56^{lck}$complex and targeting of CD4 to lysosomes. Virology 1999;257:208–219.
14. Swann SA, Williams M, Story CM, Bobbitt KR, Fleis R, and Collins KL: HIV-1 Nef blocks transport of MHC class I molecules to the cell surface via a PI 3-kinase-dependent pathway. Virology 2001;282:267–277.
15. Glushakova S, Munch J, Carl S, Greenough TC, Sullivan JL, Margolis L, and Kirchhoff F: CD4 down-modulation by human immunodeficiency virus type 1 Nef correlates with the efficiency of viral replication and with $CD4^+$ T-cell depletion in human lymphoid tissue *ex vivo*. J Virol 2001;75:10113–10117.
16. Lundquist CA, Tobiume M, Zhou J, Unutmaz D, and Aiken C: Nef-mediated downregulation of CD4 enhances human immunodeficiency virus type 1 replication in primary T lymphocytes. J Virol 2002;76:4625–4633.
17. Casartelli N, Di Matteo G, Potesta M, Rossi P, and Doria M: CD4 and major histocompatibility complex class I downregulation by the human immunodeficiency virus type 1 nef protein in pediatric AIDS progression. J Virol 2003;77:11536–11545.
18. Cortes MJ, Wong-Staal F, and Lama J: Cell surface CD4 interferes with the infectivity of HIV-1 particles released from T cells. J Biol Chem 2002;277:1770–1779.
19. Christiane F, Stroka DM, Badrichani AZ, Cooper JT, Wrighton CJ, Soares M, Grey ST, and Bach FH: A20 inhibits NF-κB activation in endothelial cells without sensitizing to tumor necrosis factor–mediated apoptosis. Blood 1998;91:2249–2258.
20. Heyninck K, De Valck D, Vanden Berghe W, Van Criekinge W, Contreras R, Fiers W, Haegeman G, and Beyaert R: The zinc finger protein A20 inhibits TNF-induced NF-κB–dependent gene expression by interfering with an RIP- or TRAF2-mediated transactivation signal and directly binds to a novel NF-κB inhibiting protein ABIN. J Cell Biol 1999;145: 1471–1482.
21. Lee EG, Boone DL, Chai S, Libby SL, Chien M, Lodolce JP, and Ma A: Failure to regulate TNF-induced NF-κB and cell death responses in A20-deficient mice. Science 2000;289:2350–2354.
22. Klinkenberg M, Van Huffel S, Heyninck K, and Beyaert R: Functional redundancy of the zinc fingers of A20 for inhibition of NF-κB activation and protein-protein interactions. FEBS Lett 2001; 498:93–97.
23. Yamamoto Y, and Gaynor RB: IκB kinases: key regulators of the NF-κB pathway. Trends Biochem Sci 2004;29:72–79.
24. Beyaert R, Heyninck K, and Van Huffel S: A20 and A20-binding proteins as cellular inhibitors of nuclear factor-κB-dependent gene expression and apoptosis. Biochem Pharmacol 2000;60: 1143–1151.
25. Heyninck K, Kreike MM, and Beyaert R: Structure-function analysis of the A20-binding inhibitor of NF-κB activation, ABIN-1. FEBS Lett 2003;536:135–140.
26. Gallagher J, Howlin J, McCarthy C, Murphy EP, Bresnihan B, FitzGerald O, Godson C, Brady HR, and Martin F: Identification of Naf1/ABIN-1 among TNF-α–induced expressed genes in human synoviocytes using oligonucleotide microarrays. FEBS Lett 2003;551:8–12.
27. El Bakkouri K, Wullaert A, Haegman M, Heyninck K, and Beyaert R: Adenoviral gene transfer of the NF-κB inhibitory protein ABIN-1 decreases allergic airway inflammation in a murine asthma model. J Biol Chem 2005;280:17938–17944.
28. Zhang S, Fukushi M, Hashimoto S, Gao C, Huang L, Fukuyo Y, Nakajima T, Amagasa T, Enomoto S, Koike K, Miura O, Yamamoto N, and Tsuchida N: A new ERK2 binding protein, Naf1, attenuates the EGF/ERK2 nuclear signaling. Biochem Biophys Res Commun 2002;297:17–23.
29. Massotte D, Baroche L, Simonin F, Yu L, Kieffer B, and Pattus F: Characterization of δ, κ, and μ human opioid receptors overexpressed in baculovirus-infected insect cells. J Biol Chem 1997;272: 19987–19992.
30. Kozasa T, and Gilman AG: Purification of recombinant G proteins from Sf9 cells by hexahistidine tagging of associated subunits. Characterization of α_{12} and inhibition of adenylyl cyclase by α_z. J Biol Chem 1995;270:1734–1741.
31. Grennan Jones F, Wolstenholme A, Fowler S, Smith S, Ziemnicka K, Bradbury J, Furmaniak J, and Rees Smith B: High-level expression of recombinant immunoreactive thyroid peroxidase

in the High Five insect cell line. J Mol Endocrinol 1996; 17:165–174.
32. Nelson PN, Reynolds GM, Waldron EE, Ward E, Giannopoulos K, and Murray PG: Monoclonal antibodies. Mol Pathol 2000;53:111–117.
33. Horiuchi S, Ampofo W, Koyanagi Y, Yamashita A, Waki M, Matsumoto A, Yamamoto M, and Yamamoto N: High-level production of alternatively spliced soluble interleukin-6 receptor in serum of patients with adult T-cell leukaemia/HTLV-I–associated myelopathy. Immunology 1998;95:360–369.
34. Rabilloud T, Vuillard L, Gilly C, and Lawrence JJ: Silver-staining of proteins in polyacrylamide gels: a general overview. Cell Mol Biol 1994;40:57–75.
35. Na BK, Chung GT, and Song CY: Production, characterization, and epitope mapping of a monoclonal antibody against aspartic proteinase of *Candida albicans*. Clin Diagn Lab Immunol 1999;6: 429–433.

Address reprint requests to:
Naoki Yamamoto, M.D., Ph.D.
Department of Molecular Virology
Bio-Response
Graduate School of Medicine
Tokyo Medical and Dental University
1-5-45, Yushima, Bunkyo-ku
Tokyo 113-8519, Japan

E-mail: yamamoto.mmb@tmd.ac.jp

Received for publication June 17, 2005. Accepted for publication July 14, 2005.

J. Biochem. **138**, 583–592 (2005)
doi:10.1093/jb/mvi158

Solution RNA Structures of the HIV-1 Dimerization Initiation Site in the Kissing-Loop and Extended-Duplex Dimers

Seiki Baba[1], Ken-ichi Takahashi[1,2], Satoko Noguchi[1], Hiroshi Takaku[1], Yoshio Koyanagi[3], Naoki Yamamoto[4] and Gota Kawai[1,*]

[1]Department of Life and Environmental Sciences, Chiba Institute of Technology, 2-17-1 Tsudanuma, Narashino, Chiba 275-0016; [2]Department of Bioscience, Faculty of Bioscience, Nagahama Institute of Bio-Science and Technology, 1266 Tamura-cho, Nagahama, Shiga 526-0829; [3]Institute for Virus Research, Kyoto University, Kyoto 606-8507; and [4]AIDS Research Center, The National Institute of Infectious Diseases, Toyama 1-23-1, Shinjuku-ku, Tokyo 162-8640

Received April 27, 2005; accepted August 13, 2005

Dimer formation of HIV-1 genomic RNA through its dimerization initiation site (DIS) is crucial to maintaining infectivity. Two types of dimers, the initially generated kissing-loop dimer and the subsequent product of the extended-duplex dimer, are formed in the stem-bulge-stem region with a loop including a self-complementary sequence. NMR chemical shift analysis of a 39mer RNA corresponding to DIS, DIS39, in the kissing-loop and extended-duplex dimers revealed that the three dimensional structures of the stem-bulge-stem region are extremely similar between the two types of dimers. Therefore, we designed two shorter RNA molecules, loop25 and bulge34, corresponding to the loop-stem region and the stem-bulge-stem region of DIS39, respectively. Based upon the chemical shift analysis, the conformation of the loop region of loop25 is identical to that of DIS39 for each of the two types of dimers. The conformation of bulge34 was also found to be the same as that of the corresponding region of DIS39. Thus, we determined the solution structures of loop25 in each of the two types of dimers as well as that of bulge34. Finally, the solution structures of DIS39 in the kissing-loop and extended-duplex dimers were determined by combining the parts of the structures. The solution structures of the two types of dimers were similar to each other in general with a difference found only in the A16 residue. The elucidation of the structures of DIS39 is important to understanding the molecular mechanism of the conformational dynamics of viral RNA molecules.

Key words: DIS, HIV-1, NMR, RNA, structure.

Abbreviations: DIS, dimerization initiation site; HIV-1, human immunodeficiency virus type 1.

Two molecules of viral genomic RNA are packaged in a dimeric state in the virion of human immunodeficiency virus type 1 (HIV-1), and this dimer formation is crucial to maintaining their infectivity (*1–4*). Accumulating evidence from both *in vivo* and *in vitro* experiments has shown that the specific sequence, the dimerization initiation site (DIS) located close to the 5′ terminus of the genomic RNA, is required for spontaneous dimerization of HIV-1 RNA. DIS can form a stem-loop structure with a self-complementary sequence in the loop and a bulge in the stem (*5*, *6*). The dimerization of DIS forms the kissing-loop dimer as the first step; then, their intramolecular stems are converted into intermolecular stems, generating the extended-duplex dimer (*7*, *8*). This two step dimerization process is called the kissing-loop mechanism. The kissing-loop dimer is converted into the extended-duplex dimer by incubation at 55°C (*9*, *10*) or by incubation at physiological temperature with the HIV-1 nucleocapsid protein, NCp7, which includes two basic regions and two zinc-fingers (*11*). A number of experiments have been performed to gain an understanding of the role of the zinc-fingers as well as the basic regions (*12–16*). Our previous results show that, for the two step dimerization from the kissing-loop dimer to the extended-duplex dimer, the two basic regions surrounding the N-terminal zinc finger of NCp7 have RNA chaperone activity by themselves, and the zinc fingers increase the efficiency of the activity (*17*, *18*).

A number of three dimensional structural analyses using NMR and X-ray methods have been performed to determine the conformation of each region of DIS, the loop region in the kissing-loop (*19*, *20*) or extended-duplex dimers (*21–24*), as well as the bulge-out region (*25–27*). However, our previous studies suggested that the 39mer RNA sequence, DIS39, which covers the entire bulge and loop regions, is necessary and sufficient for the two step dimerization (*28*, *29*). Thus, it is still relevant to determine the structures of the kissing-loop and extended-duplex dimers for DIS39 with the same sequence and conditions.

In the present study, we designed two shorter RNA molecules, loop25 and bulge34; loop25 includes the loop-stem region of DIS39, and bulge34 includes the stem-bulge-stem region (Fig. 1), respectively we then determined the solution structures of loop25 in each of the kissing-loop and extended-duplex dimers as well as bulge34. By combining the structure parts, the solution structures of DIS39 in the kissing-loop and extended-duplex dimers were able to be determined.

*To whom correspondence should be addressed. Tel/Fax: +81-47-478-0425, E-mail: gkawai@sea.it-chiba.ac.jp

 © 2005 The Japanese Biochemical Society.

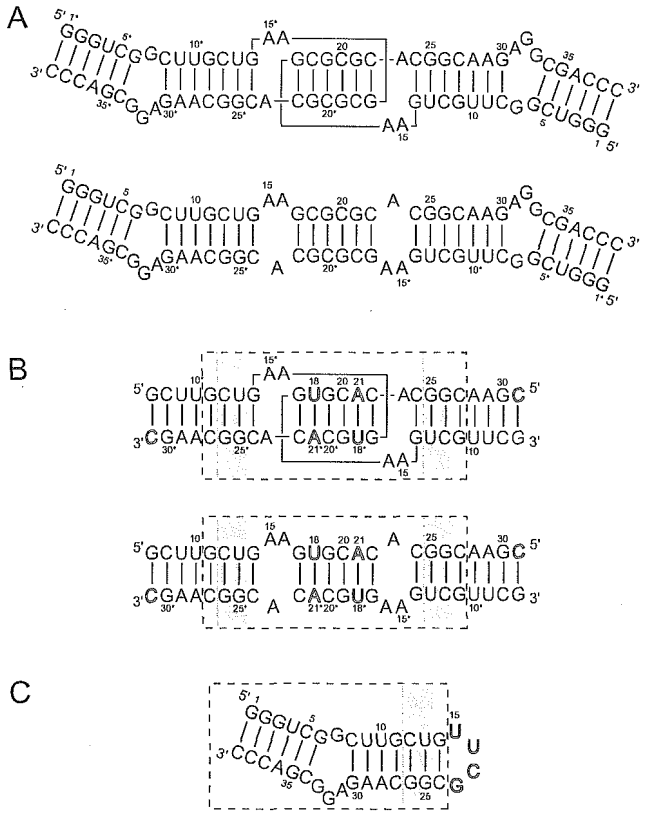

Fig. 1. **Secondary structure of a 39mer RNA corresponding to the dimerization initiation site (DIS39) and its fragments used in this study.** (A) The kissing-loop and extended-duplex dimers of DIS39. (B) The kissing-loop and extended-duplex dimers of loop25, which is composed of the loop and stem of DIS39. Modified residues are indicated by open characters. The sequence of the self-complementary loop was modified to increase the dispersion of NMR signals, and a base pair was added to the stem. The broken box indicates the part to be used for structure calculation. (C) Bulge34 consists of the stem-bulge-stem region of DIS39 and the connecting UUCG loop. The broken box indicates the part to be used for structure calculation. Gray shading indicates the two base pairs, C12–G26 and U13–G25, that are superimposed to combine the structures of the kissing-loop or extended-duplex dimer region and the stem-bulge-stem region. Asterisks indicate residues in the other strand.

MATERIALS AND METHODS

RNA Synthesis, Purification and Preparation—Non-labeled loop25 was synthesized chemically by the phosphoramidite method with an automatic DNA/RNA synthesizer, Expedite model 8909 (PerSeptive Biosystems Inc., MA, USA). The protection groups were removed with ammonia and tetra-*n*-butylammonium fluoride. Non-labeled DIS39 and bulge34 were synthesized enzymatically by the *in vitro* transcription reaction method with AmpliScribe T7 transcription kits (Epicentre Technologies Co., WI, USA). Purification for each RNA sample was performed by PAGE using 30 cm × 40 cm glass plates (Nihon Eido Co. Ltd., Tokyo, Japan) under denaturing conditions, and extensive desalting by ultrafiltration (Centricon YM3, Amicon Inc., MA, USA) was carried out. For stable isotopic labeling by the *in vitro* transcription with ^{13}C- and ^{15}N-labeled NTPs (Nippon Sanso, Tokyo, Japan), we used DIS39 rather than shorter loop25 and bulge34 because the efficiency of *in vitro* transcription is better for larger RNA.

For the preparation of the kissing-loop dimer, DIS39 or loop25 in water was incubated at 368 K for 5 min and chilled on ice for 5 min. Then, the solvent was adjusted to 1× PN-buffer [10 mM sodium phosphate (pH 7.0) and 50 mM NaCl] by adding concentrated buffer. For the preparation of the extended-duplex dimer, DIS39 or loop25 in 1× PN-buffer was incubated at 368 K for 5 min and slowly cooled to room temperature. Bulge34 was annealed by heating at 363 K for 5 min and snap-cooling on ice. To confirm the formation of the hairpin structure, the samples were subjected to a native PAGE experiment. For NMR measurements, RNA samples were dissolved in 10 mM sodium phosphate buffer (pH 7.0) containing 50 mM NaCl. The final concentration of chemically synthesized loop25 was 1.8 mM. The concentrations of DIS39 and bulge34 (transcripts) were 1.0 and 0.5 mM, respectively. The concentration of the kissing-loop and extended-duplex dimers of [G-^{13}C/^{15}N] and [A-^{13}C/^{15}N] DIS39 were 0.4, 0.3, 0.2 and 0.1 mM, respectively.

NMR Measurements—NMR spectra were recorded on Bruker DRX-500 and DRX-600 spectrometers. Spectra were recorded at probe temperatures of 283 to 303 K and NMR data at 298 K were used for structure calculation. The imino proton signal of the G and U residues in H_2O were distinguished from each other by the HSQC selected and HSQC filtered 1D spectra measured with ^{13}C and ^{15}N-labeled DIS39. Exchangeable proton NOEs were determined by 2D NOESY in H_2O with a mixing time of 150 ms using the jump-and-return scheme and gradient pulses for water suppression. For resonance assignments, well-established procedures were used (*30*). The H2 protons of adenosine were assigned based on a 2D HSQC experiment with natural abundance ^{13}C. NOE distance restraints from non-exchangeable protons were obtained from 2D NOESY experiments (mixing times of 50, 100, 200, and 400 ms) in D_2O. The intensities of the NOEs between exchangeable protons were interpreted as distances of 2.1–5.0 Å. For loop25, distances were estimated by analyzing the initial slope of NOE intensities for mixing times of 25, 50, 100, 200 ms. Judgment of intermolecular NOE is described in the result section. Two restraints (>5 Å) were added to the distance restraints based on the absence of NOE cross peaks in the case of the kissing-loop dimer. For bulge34, the intensities of NOEs due to nonexchangeable protons were interpreted as distances with a margin of −1.5 to +1.5 Å for the 100 ms 2D NOESY and −1.0 to +2.0 Å for the 200 ms 2D NOESY. Two restraints (>5 Å) were added to the distance restraints based on the absence of NOE cross peaks. The formation of hydrogen binding of G:C, A:U or G:U base pairs is interpreted as distance constraints as 1.8–2.1 Å for hydrogen and acceptor atoms and 2.8–3.2 Å for donor and acceptor atoms; G11:C27 to G14:C24, G11*:C27* to G14*:C24* and G17:C22* to C22:G17* for loop25 in the kissing-loop dimer, G11:C27* to G14:C24*, G11*:C27 to G14*:C24 and G17:C22* to C22:G17* for loop25 in the extended-duplex dimer, and G1:C39 to C5:G35 and U9:A29 to G14:C24 for bulge34. Dihedral restraints were obtained as described below. The absence of crosspeaks between H1′–H2′ in the 2D TOCSY and DQF-COSY experiments was interpreted as the residue being in the C3′-*endo*

conformation. On the other hand, the presence of strong crosspeaks between H1′–H2′ in the 2D TOCSY and DQF-COSY experiments was interpreted as the residue being in the C2′-*endo* conformation. The correction of sugar puckering is interpreted as dihedral restraints for ν_2 as 40.00 ± 20.00° (C3′-*endo*) or −35.00 ± 20.00° (C2′-*endo*). Based on the sequential connectivity of the Watson-Crick and G-U base pairs, the RNA-A conformation was assumed for the stem region and dihedral restraints were introduced for backbone torsion angles (α, β, γ, δ, ε and ζ) as the ideal conformation with a margin of ±10.00°. For loop25 in the kissing-loop dimer, information about the C3′-*endo* conformation (G11–G14, G17–C27), the C2′-*endo* conformation (A16) and RNA-A conformation in the stem region (G11–U13, U18–A21, G25–C27) was used as the dihedral restraints. For loop25 of the extended-duplex dimer, information about the C3′-*endo* conformation (G11–G14, G17-C27) and RNA-A conformation in the stem region (G11–U13, U18–A21, G25–C27) was used as the dihedral restraints. For bulge34, the information about the C3′-*endo* conformation (G1–G14, C24–A31, C34–C39) and RNA-A conformation in the stem region (G1–C5, G11–G14, C24–C27, G35–C39) was used as the dihedral restraints.

Structure Calculation—A set of 100 structures was calculated using the simulated annealing protocol described below with the InsightII/Discover package, and the amber force field was used. The force constants were 100 kcal mol^{-1} $Å^{-2}$ for distance restraints and 100 kcal mol^{-1} rad^{-2} for dihedral restraints. The starting coordinates were randomized, and the randomized structures were heated to 2,000 K in 5 ps, and the temperature was kept to 2,000 K for another 5 ps. After that, all restraints were increased to full values in 20 ps, then, decreased to 1/10 of full values in 5 ps at 2,000 K. Van der Waals radii were increased from 0.1 to 0.825 in 20 ps at 2,000 K. All restraints were increased to full value again in 10 ps at 2,000 K. Scalings for non-bond interactions were increased to full value in the next 20 ps at 2,000 K, and the temperature was kept to 2,000 K for another 5 ps. Then, the temperature was gradually scaled to 300 K in 10 ps. After that, the structure was heated from 300 to 1,000 K in 5 ps, and the van der Waals radii were increased from 0.825 to 1 at 1,000 K, and then decreased from 1 to 0.825 at 1,000 K. An additional 5 ps of dynamics was performed at 1,000 K, and the temperature was gradually scaled to 300 K for 10 ps. A final minimization step was performed, which included a Lennard-Jones potential and electrostatic terms with a dielectric constant of 7. The ten final structures with the lowest total energies were chosen.

RESULTS AND DISCUSSION

Analysis of the NMR Spectra of DIS39, Loop25 and Bulge34—Our previous NMR study revealed that the two types of dimers of DIS39 prepared as described in "MATERIALS AND METHODS" correspond to the kissing-loop and extended-duplex dimers (*31*). NMR spectra of DIS39 in each of the kissing-loop and extended-duplex dimers were measured in D_2O, and the signals due to H1′, H6/H8 were assigned by the sequential assignment method (Fig. 2). Figure 3A shows the difference in the chemical shift of H1′, H6/H8 between the two types of dimers. It was found that the difference is concentrated in the loop region. Interestingly, structures of the stem-bulge-stem region of the kissing-loop and extended-duplex dimers were extremely similar, even though the stems are formed by intra and inter molecules. This was also shown by analysis of the TOCSY spectrum; differences are located in the loop regions. Most residues were adapted to the C3′-*endo* conformation except for G32, G33 in the bulge-out region of both forms, A16 in the kissing-loop dimer and A15, A16 in the extended-duplex dimer, which might be a mixture of the C2′-*endo* and C3′-*endo* conformations.

To reveal further authentic structure, two RNA molecules were designed; loop25 includes the loop region and bulge34 includes the stem-bulge-stem region (Fig. 1, B and C). Loop25 was constructed to determine the authentic structure of the loop region. In order to increase the dispersion of the NMR signals, the sequence of the loop was modified from GCGCGC to GUGCAC. One base pair was added by replacing A31 by C31 in the stem to increase the stability of the kissing-loop dimer. It is noted that the loop sequences of GCGCGC and GUGCAC correspond to those of HIV-1 subtypes B and F (*32*), respectively, and both sequences have dimerization activity (*6*, *9*, *10*). The chemical shifts of loop25 were compared with those of DIS39 in each of the kissing-loop and extended-duplex dimers (Fig. 3, B and C). For both conformations, the chemical shifts for most of the stem region and A15, A16 and A23 were strikingly similar between the loop25 and DIS39. Due to the base alterations, the chemical shifts of the self complement loop were slightly different for both dimers. The chemical shift of H8 was shifted more than 0.2 ppm due to the addition of the terminal base pair. It is noteworthy that the chemical shift difference in loop25 between the kissing-loop and extended-duplex dimers (Fig. 3D) was almost identical to that of DIS39 (Fig. 3A). These results indicate that the structures of loop25 in the kissing-loop and extended-duplex dimers are essentially identical to those of DIS39. Upon analysis of the TOCSY spectrum, it was found that most of the residues were adapted to the C3′-*endo* conformation except A15 and A16 for the extended duplex dimer and A16 for the kissing loop dimer, and these results also agree with the results for DIS39.

Bulge34 was constructed to determine the authentic structure of the stem-bulge-stem region. Bulge34 consists of the stem-bulge-stem region of DIS39 and the connecting UUCG loop. The NMR signals of bulge34 were assigned by the sequential assignment technique. The chemical shift of H1′, H6/H8 of bulge34 were compared to those of DIS39 in the kissing-loop dimer (Fig. 3E). The chemical shifts for the stem-bulge-stem regions of bulge34 and DIS39 were identical, although the chemical shifts of the residues adjacent to the loop were slightly different by reflecting the difference in the closing loop sequences. Upon analysis of the TOCSY spectrum, it was found that most residues were adapted to the C3′-*endo* conformation except for G32, G33 in the bulge-out region and C in the UUCG loop, and that the conformation in the stem-bulge-stem region also agreed with that of DIS39. These results indicate that the structure of the stem-bulge-stem region of bulge34 is identical to that of DIS39.

Thus, the structures of DIS39 for two types of dimers can be determined by determining the structures of loop25 and bulge34, and combining them.

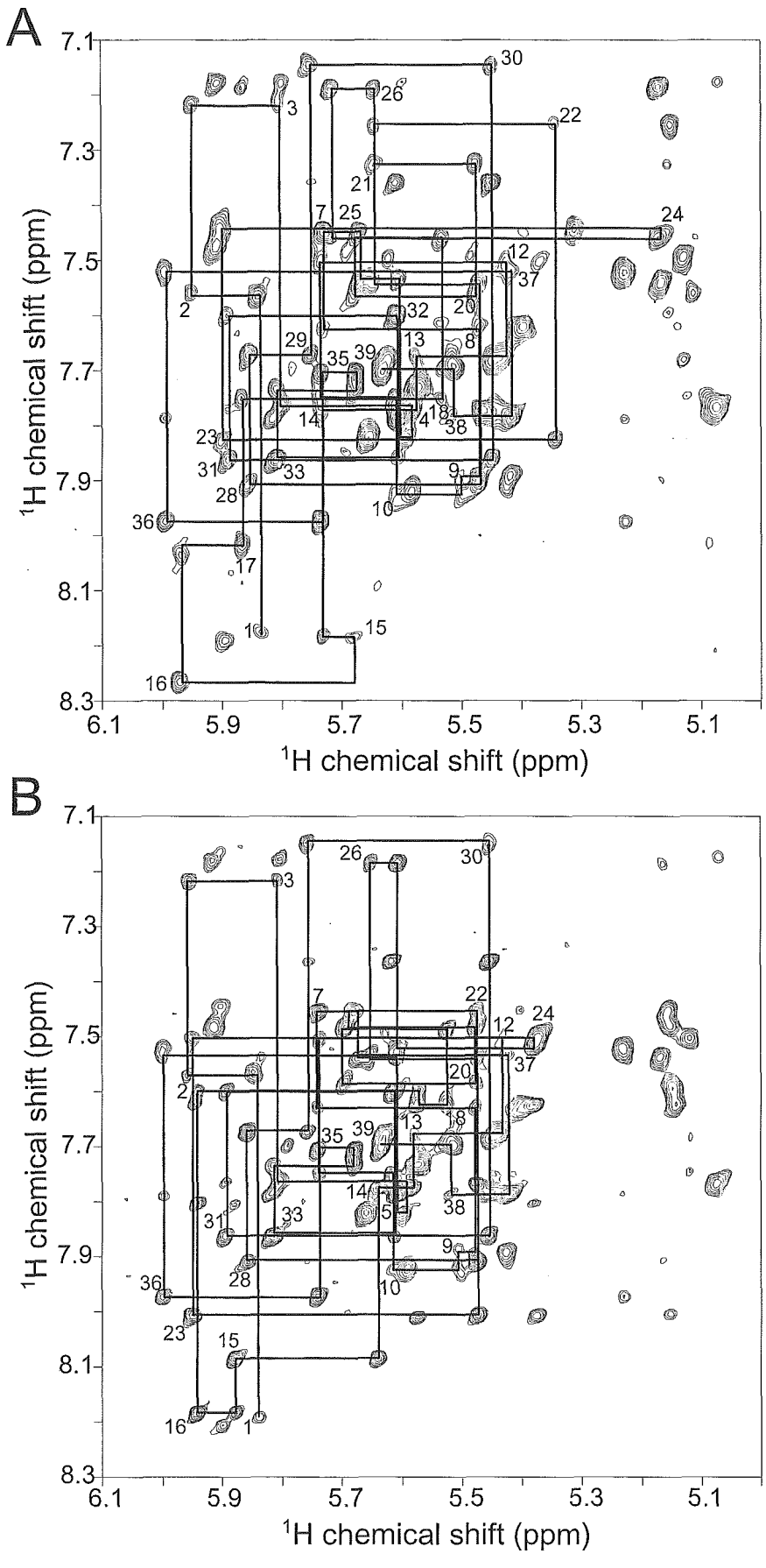

Fig. 2. **2D NOESY spectra of the (A) kissing-loop and (B) extended-duplex dimers of DIS39 measured in D_2O at 25°C with a mixing time of 200 ms.** Cross-peaks between aromatic H6/H8 protons and ribose H1′ protons are shown, and the sequential NOE connectivity is indicated.

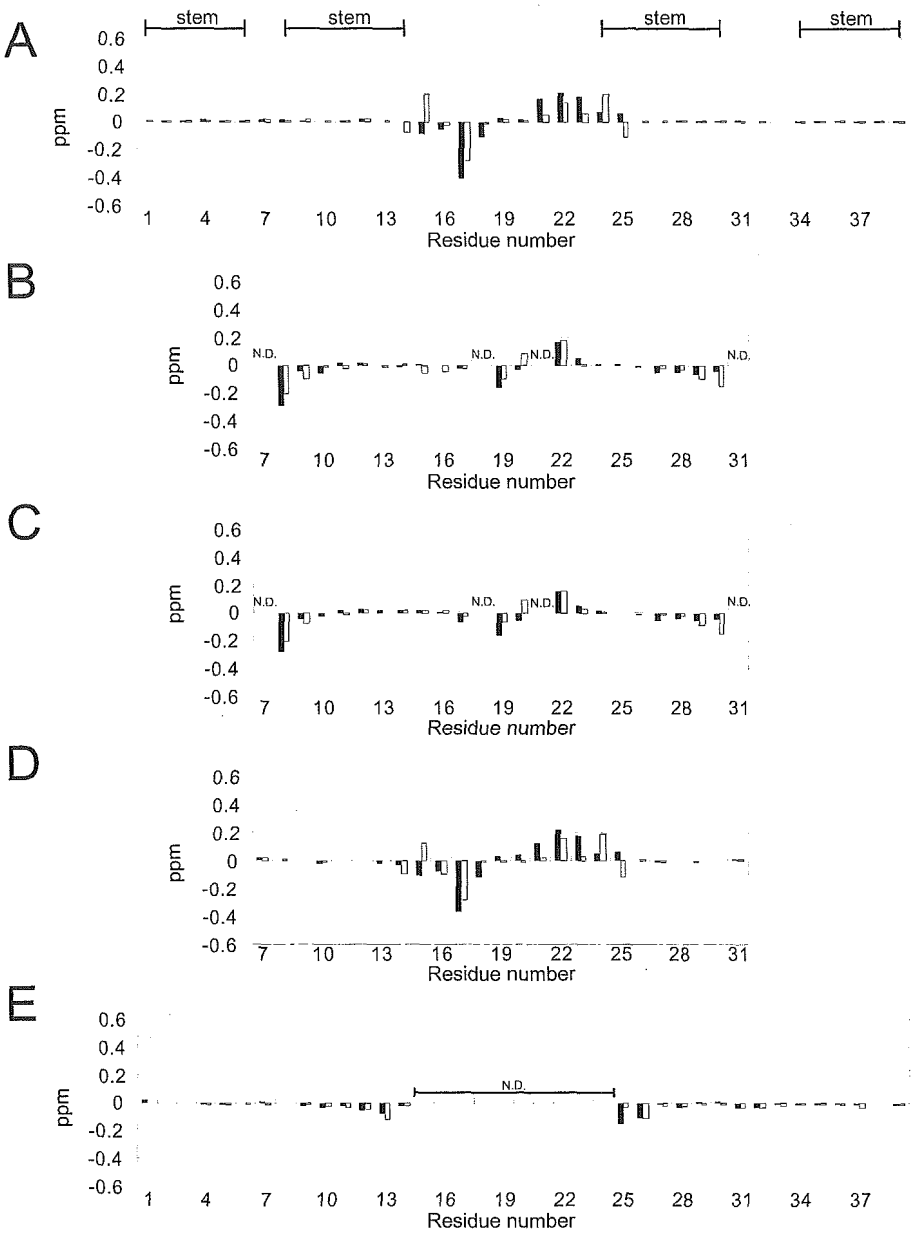

Fig. 3. **Chemical shift differences for H6/H8 and H1′.** Filled and open bars indicate H6/H8 and H1′, respectively. (A) Chemical shift differences between the kissing-loop and extended-duplex dimers of DIS39. Lines above the graph indicate the stem regions. (B) Chemical shift differences between DIS39 and loop25 in the kissing-loop dimer (data for replaced residues 7, 18, 21 and 31 are not shown). (C) Chemical shift differences between DIS39 and loop25 in the extended-duplex dimer (data for replaced residues 7, 18, 21 and 31 are not shown). (D) Chemical shift differences between the kissing-loop and extended-duplex dimers of loop25. (E) Chemical shift differences between DIS39 and bulge34 in the kissing-loop dimer (data for residues 15–24 are not shown).

Structure Determination—The loop region of loop25 in the kissing-loop dimer: To determine the structure of the loop region of DIS39 in both the kissing-loop and extended-duplex dimers, the NMR signals of loop25 were further analyzed and structural information was collected. The structure of the loop region consisting of the nine nucleotide loop and the stem with four base pairs was determined as shown by the broken box in Fig. 1B. A total of 286 distance restraints, 76 hydrogen bonding distance restraints, 140 dihedral restraints (Table 1), and 136 chiral restraints were used for the structural calculation. Three NOEs in the loop region, H2(A21)–H1′(U18), H2(A21)–H1′(G19) and H2(A21)–H8(G19), were judged to be intermolecular by analysis of the imino proton spectra. Four NOEs in the stem-loop linking region were considered to be intermolecular or intramolecular based on the results of the isotope filter NMR measurement (data not shown), and it was concluded that two NOEs, H2(A23)–H1′ (G17), H2(A16)–H1′ (G16), are intermolecular and three NOE, H8(A16)–H1′ (A16), H8(A16)–H2′ (A16), are intramolecular. One NOE in the stem-loop linking region was considered to be intermolecular or intramolecular in the structure calculation, and it was concluded that this NOE, H2(A23)–H2(A15), is intramolecular. Each restraint is used twice for two molecules. The structures were calculated by the restrained molecular dynamic calculation with the simulated annealing method. The structure was defined with a heavy atom r.m.s.d. of 2.14 Å for the ten converged structures (Fig. 4A, left panel), and the minimized average structure is shown in Fig. 4A (right panel). Although the overall convergence was not very good, the self-complementary region was well defined with 0.76 Å, and the stem-loop linking region was defined with 1.86 Å. The structural statistics are summarized in Table 1.

The loop region of loop25 in the extended-duplex dimer: The loop region of loop25 in the extended-duplex dimer was

Table 1. **NMR restraints and structural statistics.**

	Number of restraints		
	loop25 in the kissing-loop dimer (17 mer × 2)	loop25 in the extended-duplex dimer (17 mer × 2)	bulge34 (30 mer)
Distance restraints	286	384	345
imino-imino	12	12	10
intra residue	154	182	163
intra molecule	106	174	170
inter molecule	12	16	–
>5 Å	2	0	2
Hydrogen bonding distance restraints	76	76	58
Dihedral restraints	140	138	126
3′-*endo*	30	30	28
2′-*endo*	2	0	0
RNA-A stems	108	108	98
r.m.s.d. from the idealized geometry (Å)			
Bonds (Å)	0.00897 ± 0.00004	0.00803 ± 0.00020	0.00775 ± 0.00015
Angle (°)	2.43 ± 0.23	2.33 ± 0.05	2.24 ± 0.07
Impropers (°)	1.57 ± 0.10	1.82 ± 0.64	1.53 ± 0.21
Heavy-atoms r.m.s.d. (Å)[a]			
All	2.14	1.45	1.98
Stem-loop linking region[b]	1.86	1.31	
Bulge region[c]			1.90

[a]Averaged r.m.s.d. between an average structure and the 10 converged structures were calculated. The converged structures did not contain experimental distance violations >0.2 Å or dihedral violations >5°, [b]The stem-loop linking region consists of residues 14 to 17, 22 to 24, 14* to 17* and 22* to 24*, [c]The bulge region consists of residues 6 to 10 and 28 to 34. Asterisks indicate residues in the other molecule.

determined (broken box in Fig. 1B). A total of 384 distance restraints, 76 hydrogen bonding distance restraints, 138 dihedral restraints (Table 1) and 136 chiral restraints were used for the structure calculation. For the stem-loop linking region, H2 of A23 was connected by intermolecular NOEs to H1′ and H2 of A15, H2 of A16 and H1′ of G17. The structures were calculated by the restrained molecular dynamic calculation with the simulated annealing method described above. The structure was well defined with a heavy atom r.m.s.d. of 1.45 for the ten converged structures (Fig. 4B, left panel), and the minimized average structure is shown in Fig. 4B (right panel). The stem-loop linking region was defined with 1.31 Å. The structural statistics are summarized in Table 1.

The stem-bulge-stem region of bulge34: A structural determination was performed for bulge34 except for the UUCG loop (broken box in Fig. 1C). A total of 345 distance restraints, 58 hydrogen bonding distance restraints, 126 dihedral restraints (Table 1) and 120 chiral restraints were used for the structure calculation. Two NOE restraints (>5 Å), H2(A31)–H1′(U9) and H1′(A31)–H1′(U9), were added to the distance restraints based on the absence of NOE cross peaks. The structures were calculated by the restrained molecular dynamic calculation with a simulated annealing protocol. The structure was defined with a heavy atom r.m.s.d. of 1.98 for the ten converged structures (Fig. 4C, left panel), and the minimized average structure is shown in Fig. 4C (right panel). Although the overall convergence is not very good, the stem regions are well defined with 0.83 or 0.78 Å, respectively. The bulge region was defined with 1.90 Å. The structural statistics are summarized in Table 1.

The two types of dimers of DIS39: Solution structures of DIS39 were then constructed by combining the structure parts. The structures of the kissing-loop or extended-duplex dimer region and stem-bulge-stem region were combined by superimposing two base pairs, C12:G26 and U13:G25 (Fig. 1, gray area). The left panels of Fig. 5 show the ten structures prepared by using the minimized average structure of the stem-bulge-stem region (Fig. 4C, right) and each of the ten lowest energy structures of the loop region (Fig. 4, A or B, left) superimposed by the loop region. The right panels of Fig. 5 show the structures prepared using the minimized average structure of the stem-bulge-stem region (Fig. 4C, right) and the loop region (Fig. 4, A or B, right). The relative angles between the stem-bulge-stem regions differ between the kissing-loop and extended-duplex dimers as shown in the right panels of Fig. 5. However, the fluctuations of the relative angles are rather large and the ranges overlap between the two dimers as shown in the left panels of Fig. 5. In fact, the values of the residual dipolar coupling for the stem-bulge-stem region are similar between the kissing-loop and extended-duplex dimers (to be published). A preliminary normal mode analysis suggested the existence of hinge motion, and, in order to reveal the dynamic properties of the dimers, a molecular dynamics analysis, as well as the thermodynamics analysis (*33*), is required. The most obvious local difference was observed for A16; for the kissing-loop dimer, A16 was close to the same residue in the other molecule (Fig. 6A, left) and did not stack above A15 of the same molecule nor G17 of the other molecule (Fig. 6A, right), whereas for the extended-duplex dimer, A16 was apart from the same residue of the other molecule (Fig. 6B, left) and stacked between A15 and G17 (Fig. 6B, right).

Structural Comparison with Related Structures—Ennifar *et al.* (*20*) determined the crystal structure of

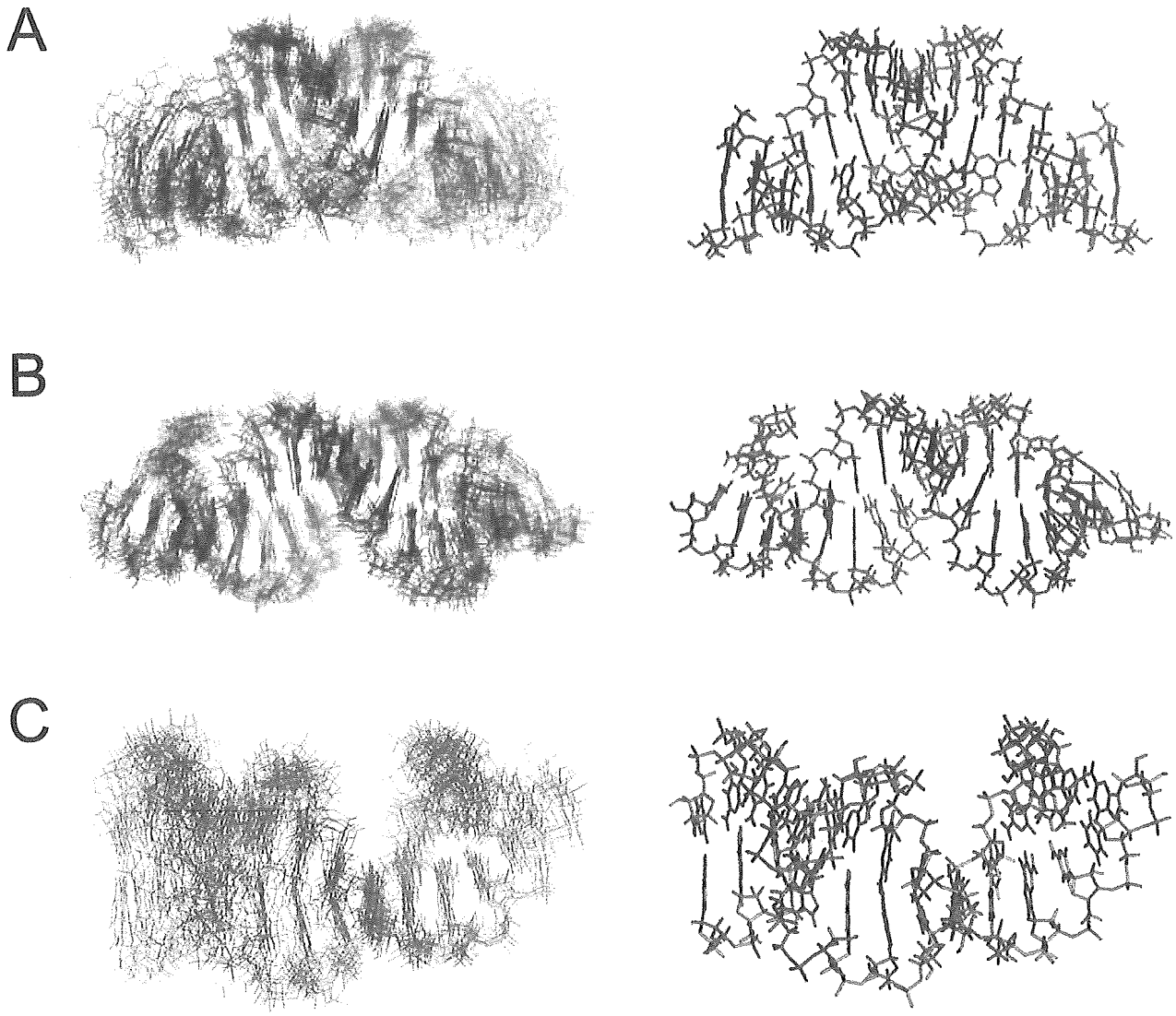

Fig. 4. **Solution structures of each part of DIS39.** Left panels show the superimposition of the 10 lowest energy structures and the right panels show the minimized average structures. (A) The loop region of loop25, as shown by the broken box in Fig. 1b, in the kissing-loop dimer. Each strand is colored in red or blue. (B) The loop region of loop25 in the extended-duplex dimer. (C) The stem-bulge-stem region of bulge34.

the kissing-loop dimer. The present structure is similar to the crystal structures in general, except for A15 and A16. In the present structure, A15 stacks on G14 and A16 interacts with the same residue in the other molecule (Fig. 6A, right). On the other hand, in the crystal structure, A15 and G16 are flipped out (*20*). It is noted that the numbering system of DIS39 is used for other structures for convenience, and position 16 is occupied by A or G depending on the strain. A15 and A16 (or G16) might be flexible and can be flipped out even in solution. Mujeeb *et al.* (*19*) determined the solution structure of the kissing-loop dimer. In this structure, A16 interacts with A15 and C24 in the other molecule, and, as a result, the distance between the two stems is relatively short. Thus, this restricted interaction makes the global structure different from the present structure and the crystal structure. However, the location of A15 is similar in the two solution structures. The difference in the conformation of A16 between the two solution structures may reflect the difference in the sequence of the stem adjacent to the loop and/or in the sample condition, including the salt concentration. The NOE connectivity determined in the present study agrees in general with those of Dardel *et al.* who analyzed the structure of the stem-loop region in the kissing-loop dimer by NMR (*34*).

Girard *et al.* (*21*) and Mujeeb *et al.* (*22*) determined the solution structures of extended-duplex dimers. In these two structures, as well as in the present structure, A15, A16 and A23 form a zipper like structure (Fig. 6B, right). On the other hand, in the case of the crystal structure of the extended-duplex dimer, G16 forms a G:A base pair and A15 is flipped out, and it was assumed that this in-out bulge transconformation is magnesium-dependent (*23*).

Structures of the stem-bulge-stem region were shown by Lawrence *et al.* (*26*) and Yuan *et al.* (*27*). In the solution structure determined by Lawrence *et al.* (*26*), continuous stackings were formed for each strand, G6-C8 and

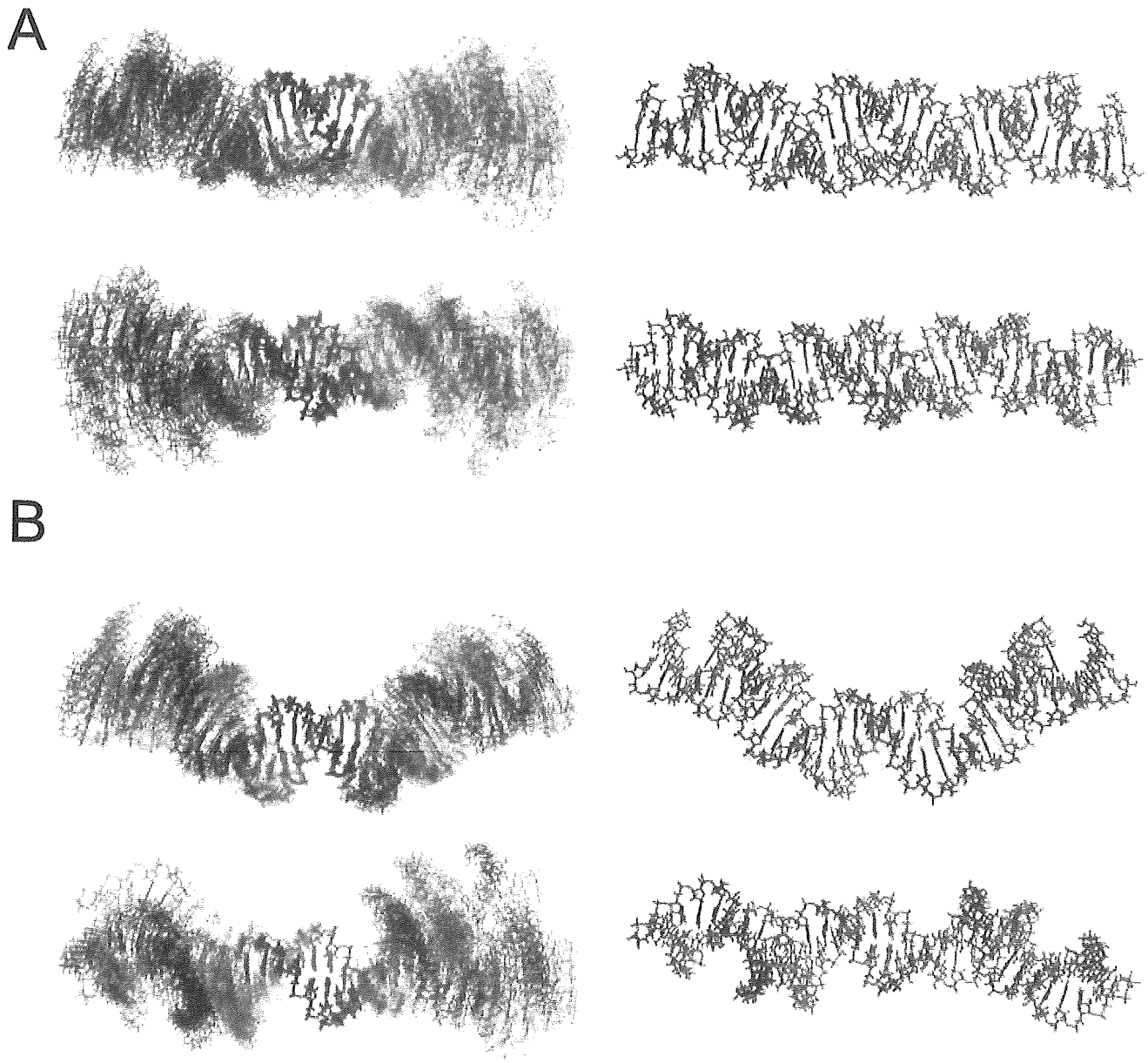

Fig. 5. **Solution structures of the (A) kissing-loop and (B) extended-duplex dimers of DIS39.** Left panels show the structures constructed by combining the structures of the loop (the 10 lowest energy structures of the kissing-loop or extended-duplex dimers) and the stem-bulge-stem (minimized average structure) regions. Right panels show the structures constructed by combining the minimized average structures of the loop and stem-bulge-stem regions. The two regions were combined by superimposing two base pairs, C12–G26 and U13–G25 (Fig. 1, gray area). Each strand is colored in red or blue and views from two different directions are shown.

G30-C34. Yuan *et al.* (*27*) showed that G7 and A31 form a base pair, and that G33 is not always stacked on G32 or C34, and, in general, the present structure is identical to the latter structure. Greatorex *et al.* (*25*) showed that the bulge region is too flexible to determine the conformation. These conformational differences may be caused by differences in the stability of the terminal stem. Lawrence *et al.* (*26*) adopted a stable 7 base-pair stem, and their structure forms an ordered conformation in the bulge region. In contrast, Greatorex *et al.* (*25*) adopted an unstable 4 base-pair stem and the bulge region is flexible. Yuan *et al.* (*27*) adopted a 4 base-pair stem and a flanking adenosine residue at the 3′ terminal that must stabilize the stem. In the present study, a 6 base-pair stem was used.

Mechanism of the Two Stem Dimerization—Between the kissing-loop and extended-duplex dimers, A16 shows the most drastic change in interaction with other residues, suggesting that A16 is the key residue in the two step dimerization reaction. The difference in the A16 conformation among structures with different sequences and determined under different conditions as described above, also suggests the importance of this residue. Mujeeb *et al.* (*19*, *22*) also pointed out the flexibility around the junction of the loop and the stem of DIS in the kissing-loop and

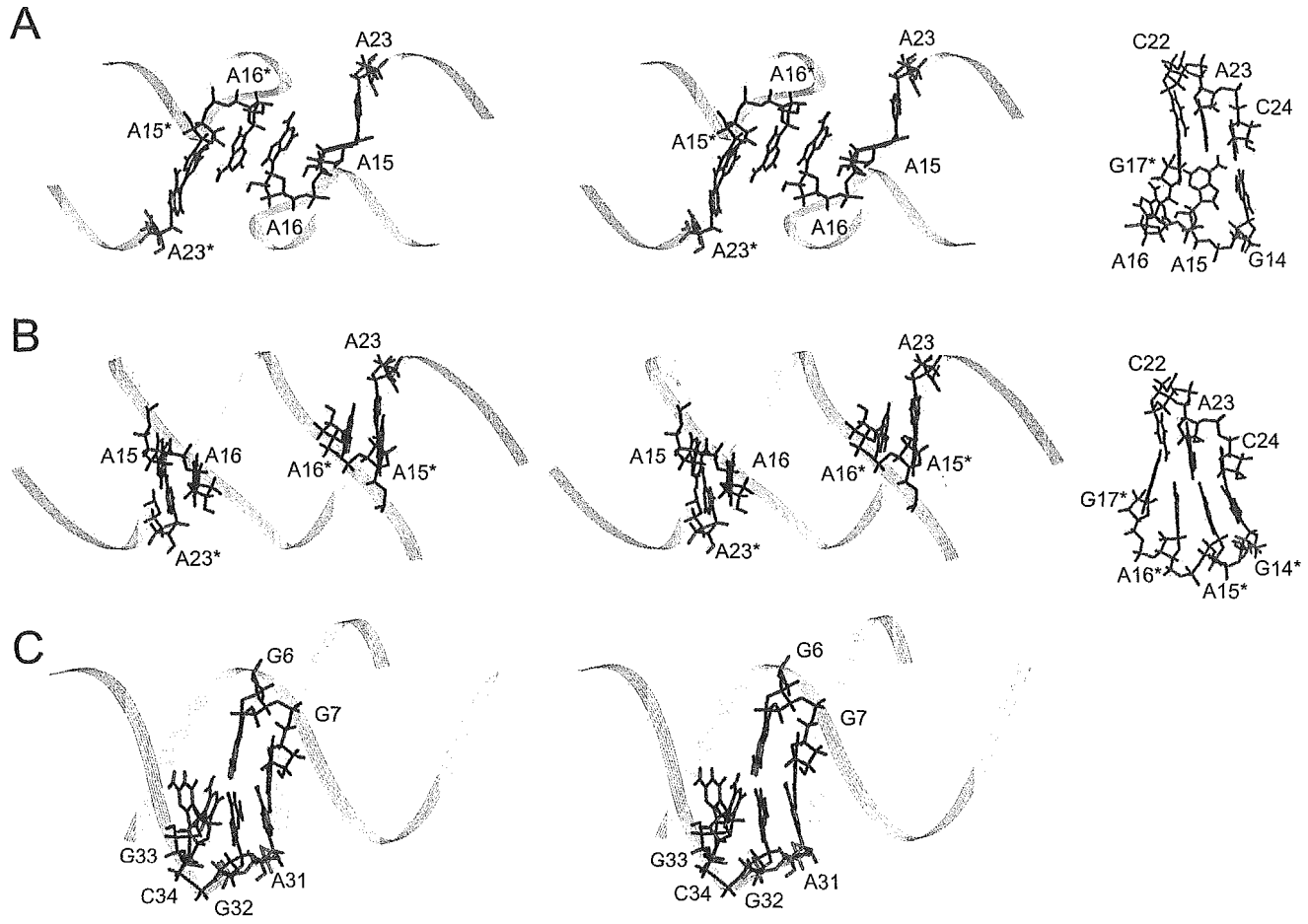

Fig. 6. **Structures of the linking regions.** (A) Regions linking the stem and loop in the kissing-loop dimer. The left panels show the positions of A15, A16, and A23 in the entire structure in a stereo view, and the right panels show residues linking the stem and loop. Asterisks indicate residues in the other strand. (B) Regions linking the stem and loop in the extended-duplex dimer. (C) The bulge region linking the two stems.

extended-duplex dimers. Imino proton signals due to U9:A29 and U10:A28 are much broader than other signals in the stem region, and no imino proton signal due to C8:G30 was observed. Thus, the stem between the loop and bulge is destabilized by the bulge region. Our previous experiments also showed that the bulge region is required for the two-step dimerization to adjust the thermal stability of DIS, and Greatorex *et al.* (*25*) also indicated that the flexibility of the bulge region is critical based on the fact that mutations in the bulge region strongly affect the melting temperature, as well as the fact that none of the wild-type sequences in the bulge region that increase the melting temperature is ever found in wild-type viruses. Thus, the conformational conversion from the kissing-loop dimer to the extended-duplex dimer might require two factors, the movement of A16 and the modest stability of the stem caused by the presence of the bulge region.

In the present study, a set of structures corresponding to the initial and final structures of the two-step dimerization of DIS are provided; these structures will promote studies to elucidate the molecular mechanism of the conformational change in the two-step dimerization, including an analysis of the interaction between DIS and NCp7, in addition to the molecular dynamics approach.

Coordinates: The structure has been deposited in the Protein Data Bank (accession code 2D17: the stem-bulge-stem region of bulge34, 2D18: the extended-duplex dimer of loop25, 2D19: the kissing-loop dimer of loop25, 2D1A: the extended-duplex dimer of DIS39 and 2D1B: the kissing-loop dimer of DIS39).

This work was supported by the "Research for the Future" Program (JSPS-RFTF97L00503) from the Japan Society for the Promotion of Science, and, in part, by a Grant-in-Aid for High Technology Research from the Ministry of Education, Science, Sports and Culture, Japan.

REFERENCES

1. Hoglund, S., Ohagen, A., Goncalves, J., Panganiban, A.T., and Gabuzda, D. (1997) Ultrastructure of HIV-1 genomic RNA. *Virology* **233**, 271–279
2. Laughrea, M., Jette, L., Mak, J., Kleiman, L., Liang, C., and Wainberg, M.A. (1997) Mutations in the kissing-loop hairpin of human immunodeficiency virus type 1 reduce viral infectivity as well as genomic RNA packaging and dimerization. *J. Virol.* **71**, 3397–3406
3. Clever, J.L. and Parslow, T.G. (1997) Mutant human immunodeficiency virus type 1 genomes with defects

in RNA dimerization or encapsidation. *J. Virol.* **71**, 3407–3414
4. Paillart, J.C., Berthoux, L., Ottmann, M., Darlix, J.L., Marquet, R., Ehresmann, B., and Ehresmann, C. (1996) A dual role of the putative RNA dimerization initiation site of human immunodeficiency virus type 1 in genomic RNA packaging and proviral DNA synthesis. *J. Virol.* **70**, 8348–8354
5. Laughrea, M. and Jette, L. (1994) A 19-nucleotide sequence upstream of the 5′ major splice donor is part of the dimerization domain of human immunodeficiency virus 1 genomic RNA. *Biochemistry* **33**, 13464–13474
6. Skripkin, E., Paillart, J.C., Marquet, R., Ehresmann, B., and Ehresmann, C. (1994) Identification of the primary site of the human immunodeficiency virus type 1 RNA dimerization *in vitro*. *Proc. Natl. Acad. Sci. USA* **91**, 4945–4949
7. Fu, W. and Rein, A. (1993) Maturation of dimeric viral RNA of Moloney murine leukemia virus. *J. Virol.* **67**, 5443–5449
8. Fu, W., Gorelick, R.J., and Rein, A. (1994) Characterization of human immunodeficiency virus type 1 dimeric RNA from wild-type and protease-defective virions. *J. Virol.* **68**, 5013–5018
9. Laughrea, M. and Jette, L. (1996) Kissing-loop model of HIV-1 genome dimerization: HIV-1 RNAs can assume alternative dimeric forms, and all sequences upstream or downstream of hairpin 248–271 are dispensable for dimer formation. *Biochemistry* **35**, 1589–1598
10. Muriaux, D., Fosse, P., and Paoletti, J. (1996) A kissing complex together with a stable dimer is involved in the HIV- 1Lai RNA dimerization process *in vitro*. *Biochemistry* **35**, 5075–5082
11. Muriaux, D., Girard, P.M., Bonnet-Mathoniere, B., and Paoletti, J. (1995) Dimerization of HIV-1Lai RNA at low ionic strength. An autocomplementary sequence in the 5′ leader region is evidenced by an antisense oligonucleotide. *J. Biol. Chem.* **270**, 8209–8216
12. Laughrea, M., Shen, N., Jette, L., Darlix, J., Kleiman, L., and Wainberg, M.A. (2001) Role of distal zinc finger of nucleocapsid protein in genomic RNA dimerization of human immunodeficiency virus type 1; No role for the palindrome crowning the R-U5 hairpin. *Virology* **281**, 109–116
13. de Guzman, R.N., Wu, Z.R., Stalling, C.C., Pappalardo, L., Borer, P.N., and Summers, M.F. (1998) Structure of the HIV-1 nucleocapsid protein bound to the SL3 ψ–RNA recognition element. *Science* **279**, 384–388
14. Amarasinghe, G.K., de Guzman, R.N., Turner, B.G., Chancellor, K.J., Wu, Z.R., and Summers, M.F. (2000) NMR structure of the HIV-1 nucleocapsid protein bound to Stem-Loop SL2 of the ψ–RNA packaging signal. Implications for Genome recognition. *J. Mol. Biol.* **301**, 491–511
15. Berkowitz, R., Fisher, J., and Goff, S.P. (1996) RNA packaging. *Curr. Top. Microbiol. Immunol.* **214**, 177–218
16. Darlix, J.L., Lopez-Lastra, M., Mély, Y., and Roques, B. (2003) Nucleocapsid protein chaperoning of nucleic acids at the heart of HIV structure, assembly and cDNA synthesis. In *HIV Sequence Compendium 2002* (Kuiken, C., Foley, B., Freed, E., Hahn, B., Marx, P., McCutchan, F., Mellors, J.W., Wolinsky, S., and Korber, B., eds.) pp. 69–88, Los Alamos National Laboratory, Los Alamos, NM
17. Takahashi, K., Baba, S., Koyanagi, Y., Yamamoto, N., Takaku, H., and Kawai, G. (2001) Two basic regions of NCp7 are sufficient for conformational conversion of HIV-1 dimerization initiation site from kissing-loop dimer to extended-duplex dimer. *J. Biol. Chem.* **276**, 31274–31278
18. Baba, S., Takahashi, K., Koyanagi, Y., Yamamoto, N., Takaku, H., Gorelick, R.J., and Kawai, G. (2003) Role of the Zinc Fingers of HIV-1 Nucleocapsid Protein in Maturation of Genomic RNA. *J. Biochem.* **134**, 637–639
19. Mujeeb, A., Clever, J.L., Billeci, T.M., James, T.L., and Parslow, T.G. (1998) Structure of the dimer initiation complex of HIV-1 genomic RNA. *Nat. Struct. Biol.* **5**, 432–436
20. Ennifar, E., Walter, P., Ehresmann, B., Ehresmann, C., and Dumas, P. (2001) Crystal Structures of Coaxially-Stacked Kissing Complexes of the HIV-1 RNA Dimerization Initiation Site. *Nat. Struct. Biol.* **8**, 1064–1068
21. Girard, F., Barbault, F., Gouyette, C., Huynh-Dinh, T., Paoletti, J., and Lancelot, G. (1999) Dimer Initiation Sequence of HIV-1Lai Genomic RNA: NMR Solution Structure of the Extended Duplex. *J. Biomol. Struct. Dyn.* **16**, 1145–1157
22. Mujeeb, A., Parslow, T.G., Zarrinpar, A., Das, C., and James, T.L. (1999) NMR structure of the mature dimer initiation complex of HIV-1 genomic RNA. *FEBS Lett.* **458**, 387–392
23. Ennifar, E., Yusupov, M., Walter, P., Marquet, R., Ehresmann, B., Ehresmann, C., and Dumas, P. (1999) The crystal structure of the dimerization initiation site of genomic HIV-1 RNA reveals an extended duplex with two adenine bulges. *Structure Fold Des.* **7**, 1439–1449
24. Ennifar, E., Walter, P., and Dumas, P. (2003) A Crystallographic Study of the Binding of 13 Metal Ions to Two Related RNA Duplexes. *Nucleic Acids Res.* **31**, 2671–2682
25. Greatorex, J., Gallego, J., Varani, G., and Lever, A. (2002) Structure and Stability of Wild-Type and Mutant RNA Internal Loops from the SL-1 Domain of the HIV-1 Packaging Signal. *J.Mol.Biol.* **322**, 543–557
26. Lawrence, D.C., Stover, C.C., Noznitsky, J., Wu, Z., and Summers, M. F. (2003) Structure of the Intact Stem and Bulge of HIV-1 Psi-RNA Stem-Loop Sl1. *J. Mol. Biol.* **326**, 529–542
27. Yuan, Y., Kerwood, D.J., Paoletti, A.C., Shubsda, M.F., and Borer, P.N. (2003) Stem of SL1 RNA in HIV-1: structure and nucleocapsid protein binding for a 1 × 3 internal loop. *Biochemistry* **42**, 5259–5269
28. Shen, N., Jette, L., Liang, C., Wainberg, M.A., and Laughrea, M. (2000) Impact of human immunodeficiency virus type 1 RNA dimerization on viral infectivity and of stem-loop B on RNA dimerization and reverse transcription and dissociation of dimerization from packaging. *J. Virol.* **74**, 5729–5735
29. Takahashi, K.I., Baba, S., Chattopadhyay, P., Koyanagi, Y., Yamamoto, N., Takaku, H., and Kawai, G. (2000) Structural requirement for the two-step dimerization of human immunodeficiency virus type 1 genome. *RNA* **6**, 96–102
30. Varani, G., Aboul-era, F., and Allain, F.H.-T. (1996) NMR investigation of RNA structure. *Prog. NMR Spect.* **29**, 51–127
31. Takahashi, K., Baba, S., Hayashi, S., Koyanagi, Y., Yamamoto, N., Takaku, H., and Kawai, G. (2000) NMR analysis on intra- and inter-molecular stems in the dimerization initiation site of the HIV-1 genome. *J. Biochem.* **127**, 681–639
32. St.Louis, D.C., Gotte, D., Sanders-Buell, E., Ritchey, D.W., Salminen, M.O., Carr, J.K., and McCutchan, F.E. (1998) Infectious molecular clones with the nonhomologous dimer initiation sequences found in different subtypes of human immunodeficiency virus type 1 can recombine and initiate a spreading infection in vitro. *J. Virol.* **72**, 3991–3998
33. Weixlbaumer, A., Werner, A., Flamm, C., Westhof, E., and Schroeder, R. (2004) Determination of thermodynamic parameters for HIV DIS type loop-loop kissing complexes. *Nucleic Acids Res.* **32**, 5126–5133
34. Dardel, R., Marguet, R., Ehresmann, C., Ehresmann, B., and Blanquet, S. (1998) Solution studies of the dimerization initiation site of HIV-1 genomic RNA. *Nucleic Acids Res.* **26**, 3567–3571

平成17年度厚生労働科学研究費補助金

エイズ対策研究事業

研究成果抄録集

（抜　粋）

エイズ対策研究事業の企画と評価に関する研究

主任研究者　　山 本 直 樹

臨床医学研究

HIV診療支援ネットワークを活用した診療連携の利活用に関する研究

課題番号：　H-17-エイズ-001
主任研究者名：　秋山昌範（国立国際医療センター医療情報システム開発研究部　部長）
分担研究者：　山本隆一（東京大学情報学環　助教授）　高橋紘士（立教大学コミュニティ福祉学部　教授）
横内清光（文教大学情報学部　教授）　木内貴弘（東京大学医学部　教授）

１．研究目的

本研究は、わが国で初めて導入された診療情報共有システムであるHIV診療支援ネットワークシステム(A-net)の導入により、全国のエイズ拠点病院においてHIV診療の標準化を行うことを最終目標に、HIV診療情報の共有化による医療連携や研究を行える体制を目指すものである。医療の分野において、情報ネットワークや広域ネットワークを利用した電子カルテ等による情報の共有化研究が行われているが、すべて実験段階であり、実際に運用している例はほとんど見られない。さらに、複数施設間でカルテを一元管理するのは国際的にも初めての試みであった。インターネットを介してセキュリティを保った状態で施設同士をつなぐ技術である仮想専用線網の研究報告も医療分野においては、ほとんど行われていなかったが、現在ではさらに安全な技術が開発されており、A-netにおけるセキュリティ技術水準は過去のものになりつつある。したがって、今までの研究や運用で判明した問題点を検討し、早急に2005年の技術水準を適応するための技術的研究開発や運用面での改善を図る必要があり、これらの調査実証を目的とする。

２．研究方法

一般に、利便性とセキュリティは相反する性格を持つといわれており、2005年4月施行の「個人情報の保護に関する法律」を踏まえ、プライバシー保護に役立つ最新のセキュリティ技術と臨床現場で利用可能な利便性がいかなるレベルで運用･維持できるかを調査し、適応するために実証する必要がある。A-netには平成17年11月現在で500症例以上が登録されている。このA-netの電子カルテは、各診療機会毎の症状のみならず、治療行為、ウイルス量などの検査結果等いわゆる臨床試験に必要なデータが、1患者1カルテとして、複数の病院を統一してすべて記録されているシステムである。一方、他の分野で広く普及している癌登録や脳卒中登録、透析患者登録といった患者登録は、年に一度程度のサマリ情報であり、受診毎のデータなど詳細なデータを集計できている訳ではない。したがってネットワーク型電子カルテを使った臨床研究応用の方策は、病院間の診療連携のみならず多施設診療研究にも応用できると考えられる。さらに、近年急速に普及してきた病院内の電子カルテとの連動も図る必要がある。すでにこれまでの研究班で、集積データを臨床研究に応用する際、患者のプライバシーを損なわない様に指針作りをする必要があることが指摘されガイドライン案が提示されたが、その後、平成16年10月29日に厚生労働省医政局総務課より「医療・介護関係事業者における個人情報の適切な取扱いのためのガイドライン（案）」が発出されており、A-netのガイドライトもこの案との整合性を図る必要が出てきた。さらに、研究利用者の拡大のために、患者の個人情報をどこまで削除すれば個人を特定できないか（無名性）の定量的検討も、すでに前述した研究班が検討していた。本研究ではその成果を踏まえ、実際のA-netシステムを活用し研究を行えるような環境づくりを検討する。また、近年急速に医療情報の電子化が推進されてきたが、未だA-net以外に大規模な臨床データが蓄積されていないのが現状である。それには、いくつかの問題点があると予想されるが、大きく分けて、技術的側面と患者の心理的側面に分けられると考えられるが、主に情報通信技術的検討を行う。

３．研究結果

現状のA-netの問題点

１）アプリケーションサーバの問題

A-netのソフトを格納・配信するサーうすの中心となるサーバであるが、老朽化により以下の問題が生じている。

①H9年度の補正予算を基に構築されたサーバで有る為、ハードウェア自体の保守廃止時期が近い将来訪れると予想される。既に一部分であるが、保守廃止対象となった機器も存在している。

②同様に導入されているソフトウェアに関してもサポート契約が廃止されており、ソフトウェアに何らかの障害が起きた際には対応することができない状況である。

③近年の技術革新によりハードウェアの性能が現時点のものと比べて劣っている。この為、ユーザからのパフォーマンスアップに対する要望が強い。

２）Virtual Private Network （ＶＰＮ：仮想専用線網）関連の問題

現在では、VPNの技術を用いてインターネットを介した安全な情報基盤の技術は既に確立されたが、A-netはわが国最初の導入であり、現在の標準的技術より、前のものとなっている。そこで、以下の問題点が生じている。

①H15年度より新規参加施設募集を休止

＜経緯＞
H10 年度より国立病院（現国立病院機構）以外の施設に導入を開始する。当時、全国規模としては世界初の事例であった。以後、VPN が世間に普及する事により、業界標準化統一への流れとなる。業界標準普及に伴い、H12 年度をもって現行使用しているIBMトンネリング方式のVPNソフトウェアーライセンスの販売を停止している。しかし、H13年度～H14年度についてはIBM内での例外処理により、特別にライセンス供給された。この2年間の間に、新しい仕組への移行について厚生労働省疾病対策課等で検討されたが結果的に移行はされずH15年度より新規参加施設募集の休止となった。
②アプリケーションサーバと同様にH10年度より導入したハードウェアの為、保守廃止時期が近い将来訪れると予想される。
③同様に導入されているソフトウェアに関してもサポート契約が廃止されており、ソフトウェアに何らかの障害が起きた際には対応することができない状況である。
④H10 年度より導入を開始したが、当時はインターネットのインフラ環境が現在のように充実（ADSL や光ケーブル）していなかった為、殆どの施設がナローバンド接続（128Kb以下の回線接続）を行っている。このため、ユーザからのパフォーマンスアップに対する要望が強い。
【参考】VPN サーバ導入年度別施設数

H10 年度	５５施設
H11 年度	１９施設
H12 年度	６施設
H13 年度	５施設
H14 年度	３施設
合計	８８施設

４．考察
HIV診療情報の共有化を図るために、A-netが構築され、現在、約130箇所のエイズ拠点病院で利用され、500例以上が患者登録され継続的に使用されており、そのデータを有効利用させる必要がある。そこで、利活用に対する問題点抽出のための現状調査を行い、主に技術的な検討を行った。この結果を踏まえ、利活用を促進するための阻害要因となっている因子をユーザや患者のサイドからは、プライバシー問題に関する認識が変わっていると予想され、来年度以降その検討も行う予定である。具体的には、A-net の受容には何が必要か、またA-net の受容を阻害する要因がどこにあるか検討を進め、「A-net」という仕組みをさらに、わかりやすく親近感のあるものへ変更する必要性が求められている。そのため、施設間を連携する仕組みで、地域連携を行っている地域の現状を調査し、上手く言っている地域とそうでない地域の比較検討を行い、A-net に応用する。また、プライバシー保護の観点から、現状の技術を応用した端末の認証レベルの向上を図るためのソフトウェアやハードウェアの研究も行い、21世紀にあるべき疾病単位の患者データベースや連携システムの提案を行う。これらの技術を応用することで、A-net 利用者以外の研究利用という二次利用拡大も図りたい。
５．自己評価
１）達成度について
A-net は、ネットワーク型電子カルテとして既に実働している希有な存在である。システムとしてはセキュリティやインターネットとの親和性が確認され、VPN を用いた運用形態を普遍的なものにした。しかし、その技術が現在の水準と比べ古くなっていることを示した。プライバシー保護に関する社会学的、心理学的要因の検討については、引き続き研究を進め、阻害要因の特定とその克服のための手法を確立する必要があると考えている。
２）研究成果の学術的・国際的・社会的意義について
医療情報学の分野において、医療情報ネットワークや電子カルテ等の研究が行われているが、実際に運用している例は少ない。さらに、複数施設間でカルテを一元管理する試みは、欧米でも行われるようになってきた。しかし、上手く行っているところは少ない。したがって、その共通する問題点を検討することは、意義が大きいと考えられる。
３）今後の展望について
A-net は、ネットワーク型電子カルテとして成功しており、来るべきユビキタス社会に向け、セキュアでより利便性の高いシステムとして発展することが望まれる。また、臨床疫学的観点からは、引き続き無名性の科学的な検証や患者側の要因の検討が必要である。現在の技術により必要な部分の改修を行うことで、患者のみならず、医療関係者や研究者に利活用されるために、今後も個人情報保護法施行を踏まえた観点で取り組む必要がある。
６．結論
A-net は、全国のエイズ拠点病院においてHIV診療の標準化を行うことを最終目標に、HIV診療情報の共有化による医療連携や研究を行える体制を目指すものであるが、1998年度に構築されたため、IT の進歩や個人情報保護法等を踏まえ、技術的に新たな問題点が生じている。本研究は、今までの研究や運用で判明した問題点を検討し、現在の技術水準を適応するための技術的研究開発や運用面での改善を図るための方策を検討する。
７．知的所有権の出願・取得状況
本研究をベースとし、「知識発見型大規模診療情報自動解析(データマイニング)システムの開発と各政策医療ネットワークへの応用に関する研究」と共同研究により、
特願2003-118496　疾病予後モデルの作成方法、このモデルを用いた疾患予後予測方法、このモデルによる予後予測装置、ならびにプログラム、記憶媒体．日本、韓国、米国出願済み。

研究課題名：免疫賦活を応用したHIV感染症の治療開発に関する研究

課題番号：H15－エイズ001
主任研究者：岡 慎一（国立国際医療センターエイズ治療・研究開発センター臨床研究開発部 部長）
分担研究者：滝口 雅文（熊本大学エイズ学研究センター・ウイルス制御分野 教授）、松下 修三（熊本大学エイズ学研究センター・病態制御分野 教授）、森内 浩幸（長崎大学大学院医歯薬学総合研究科 教授）、満屋 裕明（熊本大学医学部免疫病態学内科学第二 教授）、江川 滉二（㈱メディネット 取締役）、立川 夏夫（国立国際医療センターエイズ治療・研究開発センター 情報室長）

1. 研究目的

HAARTにより多くの患者の予後が改善された。しかし、治療が長期にわたるという点からいくつかの課題は残されている。本研究班は、これら課題克服を目的に以下の3つの柱で遂行した。（当初は、免疫再構築に対する対処も含めた４つの柱であったが、この柱は、２年目で到達度が低かったために中断とした。）

柱１：HIVに合併する悪性リンパ腫の治療法の開発

EBウイルス(EBV)によるリンパ腫が、HIV患者の予後に重大な影響を及ぼす。そこで、EBV特異的CD8T細胞を誘導する免疫療法をおこない、患者体内でのEBV特異的CD8T細胞の誘導を解析し、その効果を検討した。

柱２：現状の治療薬に対する耐性ウイルスの克服

*in vitro/in vivo*で強力な活性を有するAK602/Aplaviroc（AVC）と一連の誘導体を用いてHIV感染を阻害する具体的なメカニズム、CCR5阻害剤・ケモカインとCCR5の相互作用などの基礎的研究を進め、ケモカインを介した各種の生理作用に影響を与えないCCR5阻害剤の開発を進めた。ケモカイン・レセプターをターゲットとした新たな治療法が有効かつ安全に行えるために、ケモカイン・レセプターの発現と制御、そしてそれを介するシグナルが及ぼす影響を理解する。

柱３：免疫賦活を応用した現状の治療の進展

免疫慮法として行っている２つの臨床試験（急性期感染者に対するSTI療法、IL-2を用いた免疫賦活療法）の経過を観察した。さらに新たなHIV-1に対する免疫療法の基盤を確立するために、長期未発症者（LTNP）に高頻度に見られるHLA-B*5101が提示する４つのHIV-1特異的細胞傷害性T細胞（CTL）の誘導を、２０年間以上無治療で経過した血友病患者で検討した。新規に開発したin vitroにおける中和抗体の耐性誘導システムを用いて、これまでCell Lineでは困難であったR5ウイルスのin vitroでの中和抗体逃避ウイルスを比較的簡便に誘導し、in vivoでの耐性ウイルスの予測を行った。

2. 研究方法

柱１：HIVに合併する悪性リンパ腫の治療法の開発

過去２年間で、実際の免疫細胞療法を１卵生双生児であった２例に行った。DCワクチンを行った２例目では、EBVに対するCTLが誘導でき１年以上維持できているが、このレベルと他のHIV患者のEBVに対するCTLのレベルを比較した。さらに、今回は、この技術のHIV免疫療法への進展をにらみ、DCワクチン療法の基礎検討をおこなった。HIV患者および非感染者のPBMCをIL-2(20 IU/ml)存在下、抗HIV薬（AZT, 3TC, NFV）1 μMの存在／非存在下で培養し、形態、HIVの増殖の有無、細胞数を調べた。また新たにHIV患者２名と今まで対象とした一卵性双生児兄弟計４名の末梢血から抗HIV薬の存在下で誘導したmature DCをFACS解析により比較した。次にPBLとEBVのpeptide(A*2402 EBNA3B TYSAGIVQI)をパルスしたこのDCを用いて（５対１）、抗HIV薬とIL-2存在下でCTLを誘導し、MHC tetramer法とElispot法でpeptide特異的T細胞を解析した。一卵性双生児兄弟ではそれぞれ由来のDCとPBLを４通りに組み合わせてCTLを誘導した。

柱２：現状の治療薬に対する耐性ウイルスの克服

1) 抗HIV化合物の活性評価には試験管内での評価に加え、SCID-huマウスAIDSモデルを用いた評価系を用いた。

2) CCR5阻害剤の^{3}Hラベル体作成および複数の変異CCR5発現細胞株を作成、更に^{125}Iラベル化されたケモカイン(RANTES, MIP-1α, MIP-1β)を用いて野生株・変異CCR5との結合能やCCR5阻害剤とケモカインとの相互作用の検討を行なった。

3) ウシロドプシン結晶構造を基にCCR5の構造学的解析を行なった。更に変異CCR5とケモカイン・CCR5阻害剤との結合能の変化のデータを得てCCR5との結合様式の解析を進めた。

4) 宿主因子がCCR5の発現とHIVの感染性に及ぼす影響：健康成人またはHIV感染者のPBMCを①臍帯血由来のalpha-fetoprotein (AFP)、②乳清由来の諸成分、または③ストレス関連因子の添加・無添加で培養し、CCR5の発現を調べ（flow cytometry）、HIVのin vitro感染実験を行った。

5) CCR5 ligandsが潜伏したHIVの再活性化に及ぼす影響：HIV感染者のPBMC（CD8&CD14-depleted）培養においてRANTES (CCR5 agonist)＋少量の抗CD3抗体の刺激によるウイルス発現の有無を評価した。

柱３：免疫賦活を応用した現状の治療の進展

STI療法では、誘導されたCTLのエピトープのsequenceを行い、escape機序の解析を行った。IL-2を用いた免疫賦活療法は、臨床経過の観察を行った。

LTNPにおける４つのHLA-B*5101拘束性CTLを検出するために、これらのエピトープを結合させたHLA-B*5101テトラマーを作製し、７名の血友病患者での特異的CD8T細胞の数をフローサイトメトリーで解析した。

KD-247単クローン抗体存在下に、CCR5高発現T細胞株であるPM1/CCR5細胞を用いin vitro R5ウイルス（JR-FL）の逃避ウイルス誘導を行い、得られた逃避ウイルスの責任部位を導入したpseudotypeウイルスを作製した。

（倫理面への配慮）

本研究班の臨床試験は、「ヘルシンキ宣言」に基づいた厚生労働省の「臨床研究に係る倫理指針」に基づきプロトコールを作成し、国立国際医療センターの倫理委員会での承認「IL-2国際臨床試験（H11-J-95）、急性期患者に対するSTI臨床試験（H13-10）、エイズに伴う悪性リンパ腫に対するLAK療法(H15-162)」を得ている。

3. 研究結果

柱１：HIVに合併する悪性リンパ腫の治療法の開発

１例目は、悪性リンパ腫の悪化で免疫細胞療法の効果判定はできなかった。２例目は、DC治療開始後、EBV特異的なCTLの誘導が確認されDC投与終了後現在まで１０ヶ月このCTLが維持されている。このCTLのレベルは、HIV患者43例（非悪性リンパ腫）において末梢血PBMC10^{6}個あたりのCTL 130個であったのに対し、この例においては2160個であった。今後の免疫療法に向けて、HIV患者のPBMCを用いてmature DCを誘導した結果、４名とも抗HIV薬の存在下でもDC誘導が可能であった。また４名ともこのDC刺激でCTL誘導も可能で、